Lab on a Chip

Accepted Manuscript

This is an *Accepted Manuscript*, which has been through the Royal Society of Chemistry peer review process and has been accepted for publication.

Accepted Manuscripts are published online shortly after acceptance, before technical editing, formatting and proof reading. Using this free service, authors can make their results available to the community, in citable form, before we publish the edited article. We will replace this *Accepted Manuscript* with the edited and formatted *Advance Article* as soon as it is available.

You can find more information about *Accepted Manuscripts* in the **Information for Authors**.

Please note that technical editing may introduce minor changes to the text and/or graphics, which may alter content. The journal's standard **Terms & Conditions** and the **Ethical guidelines** still apply. In no event shall the Royal Society of Chemistry be held responsible for any errors or omissions in this *Accepted Manuscript* or any consequences arising from the use of any information it contains.
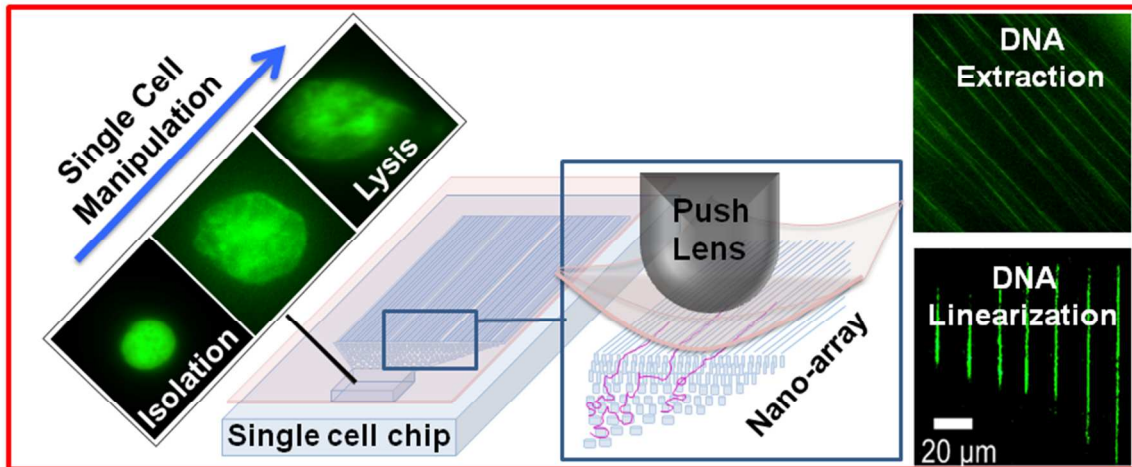
We present a lab-on-chip for next generation of single-cell genomics, performing full-cycle single-cell analysis by demonstrating mega-base pair genomic DNAs in nanochannels extracted in-situ.

ARTICLE TYPE

Development of a Platform for Single Cell Genomics Using Convex Lens-Induced Confinement

Sara Mahshid,[ab] Mohammed Jalal Ahamed,[a] Daniel Berard,[a] Susan Amin,[a] Robert Sladek,[*b] Sabrina R. Leslie,[*a‡] and Walter Reisner[*a‡]

We demonstrate a laboratory-on-chip that combines micro/nano-fabricated features with a Convex Lens-Induced Confinement (CLIC) device for the *in situ* analysis of single cells. A complete cycle of single cell analysis was achieved that includes: cell trapping, cell isolation, lysis, protein digestion, genomic DNA extraction and on-chip genomic DNA linearization. The ability to dynamically alter the flow-cell dimensions using the CLIC method was coupled with a flow-control mechanism for achieving efficient cell trapping, buffer exchange, and loading of long DNA molecules into nanofluidic arrays. Finite element simulation of fluid flow gives rise to optimized design parameters for overcoming the high hydraulic resistance present in the micro/nano-confinement region. By tuning design parameters such as the pressure gradient and CLIC confinement, an efficient on-chip single cell analysis protocol can be obtained. We demonstrate that we can extract Mbp long genomic DNA molecules from a single human lybphoblastoid cell and stretch these molecules in the nanochannels for optical interrogation.

1 Introduction

The ability to perform direct, comprehensive analysis of genomes extracted from single mammalian cells in interphase will have a significant impact in biomedical research for cancer and enhance the diagnosis of complex genetic disorders. Current approaches to identify genetic differences among individuals are based on DNA sequencing; classic metaphase or interphase karotyping; or microarray technology platforms[1–4]. DNA sequencing technologies are typically suited for detecting short variants (containing single or tens of nucleotides). Classic metaphase karotypes are suitable for identifying very large chromosomal abnormalities (involving regions ∼10-100 Mb in size). Microarrays are widely used to detect both single nucleotide polymorphisms and large structural alterations (by comparative genomic hybridization), but cannot detect changes that do not alter copy number (such as balanced translocations and inversions)[5,6]. Sequencing and microarray approaches require extensive genome fragmentation and averaging over multiple cells, obscuring the large-scale genomic organization at the level of a single cell. More-

over, these methods require molecular amplification that can introduce artifacts and obscure crucial epigenetic information. These limitations create a need for new technologies that can be used to assess genomic heterogeneity in cellular populations (such as cancers) and to perform genetic studies in situations where only a limited number of cells can be obtained (including cells isolated for pre-implantation genetic diagnosis, circulating tumor cells, or tissue biopsies).

Microfluidics-based devices and automated flow sorters have emerged as viable technologies to isolate single cells and to extract whole-cell lysates containing protein, DNA and RNA for further characterization. These have resulted in significant development of technologies that can demonstrate on-chip cell analysis[7–16]. Conventional microfluidic devices utilizing microvalves, complex fluid networks for cell handling and on-chip cell analysis can provide smaller sample volumes and faster reaction times compared to standard laboratory protocols. In parallel, there has been significant effort in developing devices to analyze single molecules of purified DNA extracted off-chip using nanofluidic and flow-based linearization[17–25]. In direct-bonded nanofluidic devices, single molecule analytes are introduced into nanochannels from adjoining microchannel reservoirs, requiring large electric or hydrodynamic forces to overcome the high free energy barriers introduced at the abrupt change in device dimensions. Development of a lab-on-a-chip single-cell device that can profile whole genomes will allow direct analysis of molecules extracted from a single cell. Compared to approaches in which the cell lysis is

[a] Address, Department of Physics, McGill University, 3600 rue University, Montreal, Canada. Fax: 514 398 8434; Tel: 514 398 3058; E-mail: reisner@physics.mcgill.ca Tel: 514 398 1835; E-mail: sabrina.leslie@mcgill.ca;

[b] Address, McGill University and Genome Quebec Innovation Centre, 740 avenue de Docteur Penfield, Montreal, Canada. Tel: 514 398 5458; E-mail: rob.sladek@mcgill.ca

‡ Prof. Reisner and Prof. Leslie are corresponding authors. To whom correspondence may be addressed. Email: reisner@physics.mcgill.ca and sabrina.leslie@mcgill.ca.
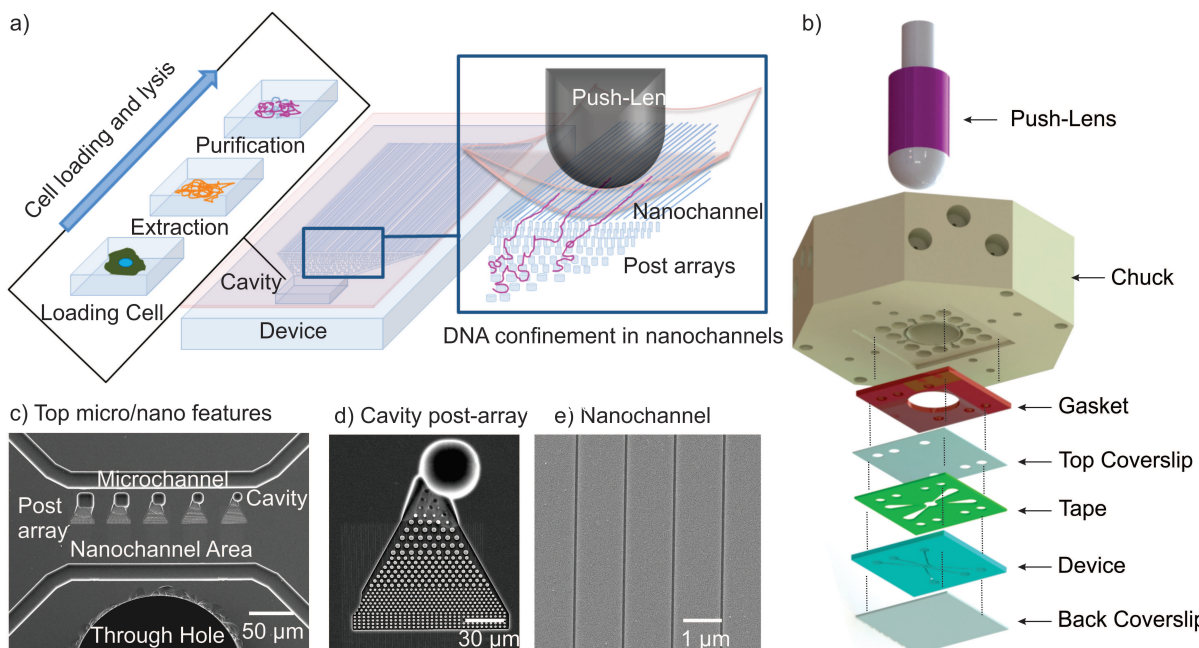
Fig. 1 (a) Schematic of cell trapping and DNA isolation by the micro-/nanofluidic lab-on-chip device incorporating Convex Lens-Induced Confinement (CLIC). The device integrates the cell trapping, lysis, DNA extraction and purification steps inside the cavity along with DNA pre-stretching in post-arrays and loading into nanochannels using CLIC. (b) 3D design showing the components of the device with respect to the CLIC push-lens. SEM images are shown for: (c) the top surface of the device, including fluidic features with respect to the position of the through-hole; (d) the etched cavity and micro-loading arrays; and (e) the array of 100 nm-etched channels in fused silica.

performed off-chip, this integrated approach could reduce genomic fragmentation due to DNA transfer (i.e. pipetting) and help ensure parallel and complete analysis of the genomic contents extracted from a single cell. However, such a device needs to operate at widely different length scales for cell isolation (microscale confinement) and DNA extension (nanoscale confinement), introducing a significant design challenge.

Here we propose a technological approach based on implementation of tunable Convex Lens-Induced Confinement (CLIC)[26–28] and micro-/nanofluidics[29] that creates a variable and tunable confinement for extracting and manipulating DNA from single cells. The variable and tunable confinement is created by locally deforming a flexible coverslip above a micro/nano-templated platform (Fig. 1a). Our device integrates the following processing steps: (a) cell handling and trapping in a microcavity; (b) metering and delivering of chemical reagents for cell lysis; (c) genomic DNA extraction and purification; (d) pre-stretching of DNA molecules in a gradient loading region; (e) transportation of DNA molecules to nanochannel arrays for extension and optical mapping. Our

approach requires no valves for cell capture and obviates the need for direct bonding. Confinement can be dynamically varied to trap a single cell, maintain the cell in the field of view throughout the lysis process and transfer the extracted DNA into nanochannel arrays. While there have been reports of microfluidic DNA extraction[7], our approach is designed specifically to isolate single cells so that DNA from a single cell, and not an ensemble of cells, can be analyzed. Our approach is also distinct from reference[21,30] in that we focus directly on interphase cells rather than metaphase chromosome preparations (which necessitate cell-culture). A recent approach[31] uses lateral confinement variation, created by squeezing of PDMS microchannels, to trap and mechanically lyse cells. We feel that the vertical confinement variation, explored here, may result in more efficient buffer exchange due to CLIC's ability to create tunable nanometric gaps that can hold a cell stationary while exposing it to continuous fluid flow.
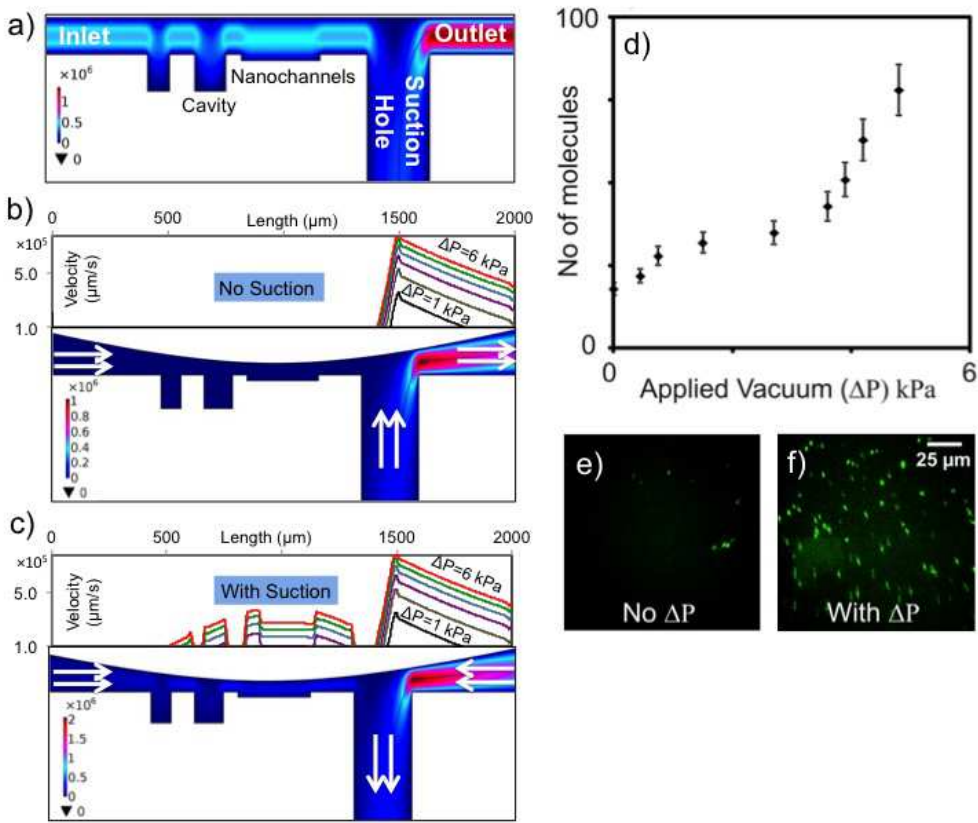
Fig. 2 Two-dimensional simulation results for fluid flow when the push-lens is (a) up and (b) down and the pressure difference is applied between the inlet microchannel and outlet microchannel reservoirs. (c) Simulation result of the fluid flow when the push-lens is down and the suction is applied via through hole near the confined area. The flow-velocity magnitude along the chamber in the b) absence and c) presence of the suction via hole is shown on top of each figure. The COMSOL geometry consists of inlet microchannel (20 μm-deep), cubic cavity (100 μm), outlet microchannels (20 μm-deep) and a central suction hole (500 μm-wide); the model is based on Stokes flow and incompressible flow with no slip-boundary conditions. d) Experimental results showing the efficiency of the suction hole for DNA accumulation in the nanoconfined region while the push-lens is down and vacuum is applied in the range of 0-6 kPa. Fluorescent image of the nanoconfined region when e) no vacuum and f) 6 kPa vacuum is applied.

2 Materials and Methods

2.1 Device Design and Fabrication

The components of the chip and CLIC instrumentation are shown in Figure 1b. The chip is placed between two coverslips: the top coverslip and the chip are separated by double-sided tape, which is laser-cut (PBS Engraving) to create channels for liquid to flow into a main central chamber, while the bottom coverslip is directly bonded to the backside of the chip[32]. The complete device assembly is mounted on the chuck using a thick silicon gasket for ease of buffer exchange. The CLIC imaging chamber is formed between the coverslip and the chip top surface, which contains embedded nano/micro fluidic features (Fig. 1a). The innovative part of our design is the existence of a through hole, close enough to the heart of the device, where the micro and nanofeatures are patterned (as shown in the SEM results of Fig. 1c). In practice, the addition of a suction-hole requires that we add a sealed fluidic layer beneath the substrate itself.

The micro/nano-fluidic fused silica device is fabricated via wafer-scale micro-fabrication technology including electron beam, contact UV lithography followed by reactive ion-etching. A 4-inch diameter fused silica wafer (Markoptics, Santa Ana, CA 500-μm thick) is used as the substrate. The first step in our process flow involves fabrication of 100-nm deep nannochannels by electron beam lithography and dry etching. A 250-μm-long and 450-μm-long array of 100-nm-wide nanochannels spaced 2-μm apart is defined using electron beam lithography (JEOL) in ZEP520A resist. The nanopatterns are then transferred to the fused silica substrate

via CF_4/CHF_3 reactive ion etching (RIE). The second step involves fabrication of micro-features via additional iterations of contact lithography and RIE, including a 20-μm deep cavity for single-cell trapping, a 20-μm deep microchannel and a 1-μm deep microloading region that can contain microposts. Etching the $\sim 10\mu$m features in glass is challenging due to the lack of efficient deep etch processes[33]. The third fabrication step is to create outlet channels and suction via-holes on the substrate backside. The outlet channels are created by a contact lithography/RIE iteration, with alignment to the top-side features being facilitated by the wafer's transparency. The suction via-holes, 150 μm in diameter, are formed by micromachining through the 500-μm thick wafer. The via-holes are aligned with a precision of less than 20 μm. Once the holes are completed, the loading reservoirs are sandblasted in the fused silica substrate. Finally, the silica wafer and coverslips are assembled. The backside of the chip is sealed using direct silica-silica bonding to a 100-μm-thick cover glass (Valley Design); and the top surface is covered with 30-μm-thick double-sided tape and attached to a coverslip with small holes sand-blasted into the corners for fluid insertion and recovery. The SEM results of the etched microcavity/post arrays and 100 nm channels are demonstrated in Fig. 1d and e.

2.2 CLIC microscope

The assembled flow chamber and chuck are mounted on the custom-built CLIC microscope for imaging[32]. The CLIC microscope is equipped with a 488 nm optically pumped semiconductor laser (Coherent Sapphire 488-150 CW CDRH). Imaging is performed on a Nikon Ti-E inverted microscope equipped with a Nikon 60x water-immersion objective (Nikon CFI Apo 60XW NIR) and an Andor iXon Ultra EMCCD camera[32]. Chemically inert PTFE tubing connects the pump outlets to the fluid entrance ports in the chuck and from the chuck to the holes in the coverslip. Syringe pumps are used to insert and retrieve the fluid from the imaging chamber, facilitating buffer exchange. The push-lens is lowered via a piezoelectric actuator (PI P-725 PIFOC, 250 μm travel range). The push-lens is lowered to deform the coverslip, creating a locally confined region. The coverslip contacts the top surface of the substrate at a single point, and the distance between the two confining surfaces gradually increases away from the center of the nanoconfined region. The chamber height profile is measured during experiments using both interferometry and fluorescence[32]. Sample heating is accomplished by heating the push-lens.

2.3 Chemicals and Materials Used

Lymphoblast cells were cultured in an incubator at 37°C in a humidified atmosphere with 5% CO_2. Cells were grown in RPMI 1640 medium supplemented with 15% FBS, 100 units/mL penicillin, 100 μg/mL streptomycin and 4 mM L-glutamine (all purchased from Life Technologies). The cell culture medium was renewed every 4 days and the cells were split into equal volumes of fresh culture media. Cells that had been subcultured more than ten times were discarded. For analysis of single cells, a 1 mL aliquot of cells was diluted using 100 mM Tris (PH 7.5) and stained with SYTO green fluorescent die (InvitrogenTM Molecular Probes) while keeping the temperature fixed at 37°C. Stained lymphoblast cells, 10-20 μm in size, were first observed under the fluorescent microscope to ensure that staining conditions are effective. The lysis and DNA extraction buffer (RIPA) is composed of 0.5-2% SDS (sodium dodecyl sulfate) in 1xTE (50 mM Tris-HCl, 1 mM EDTA, pH 8.0), 50 mM Tris-HCl[pH 8.0], 10 μg/mL DNAse-free RNAse A (Fermentas) and 5 mM CaCl_2. To ensure protein digestion during cell lysis Proteinase K (200 μg/mL) from Tritirachium album (Sigma) is added to the lysis buffer. In order to improve visualization of the extracted genomic DNA, YOYO1 (Life Technologies) is added to the lysis solution buffer at a concentration of 10 nM. Finally, 3% (vol/vol) beta-mercaptoethanol BME) was added to protect against photo bleaching. Lambda-phage DNA (48.5 kbp; New England Biosciences), at a concentration of 50 μg/mL, was used to test device operation conditions.

In ensemble experiments, where DNA from many cells are pooled, it is possible to add a precise amount of stain to a precise amount of DNA contained a precise volume of liquid and establish a known staining ratio. To achieve a 10:1 staining ratio (bp:fluor) for our λ-DNA test constructs, we use a 1.5 μM YOYO-1 concentration at a 10 μg/ml DNA concentration with a minimum incubation time of roughly one hour. While the staining ratio of the extracted genomic strands is not known precisely, we have found that the 10 nM YOYO-1 concentration used in the lysis buffer yielded uniformly stained molecules roughly comparable in brightness to the 10:1 stained λ-DNA constructs.

3 Results and Discussion

3.1 Flow actuation inside the CLIC chamber using suction hole

The flow actuation is the fundamental challenge in CLIC-based approaches due to the strong increase of hydraulic resistance with dimension. Specifically, the hydraulic resistance scales inversely with the third power of the chamber height[32]. As a result, if a pressure gradient is applied between the fluid injection ports at each side of the CLIC imaging chamber, the solution will fail to penetrate the confined area and will circulate around it. Consequently, hydrodynamic actuation cannot be used to cycle molecules through the

a) Schematic of Cell Trapping   b) Image time sequence of cell trapping
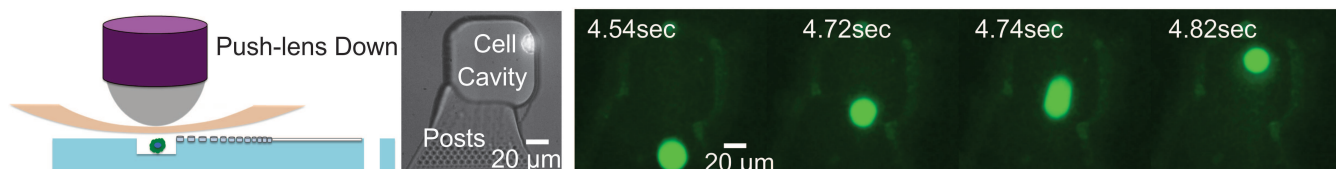
c) Position of the push-lens during cell trapping
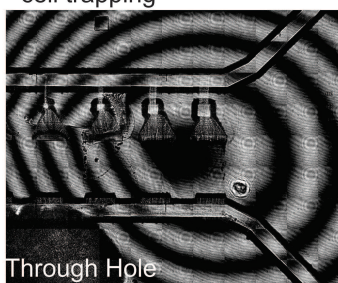
d) Coverslip deformation during cell trapping
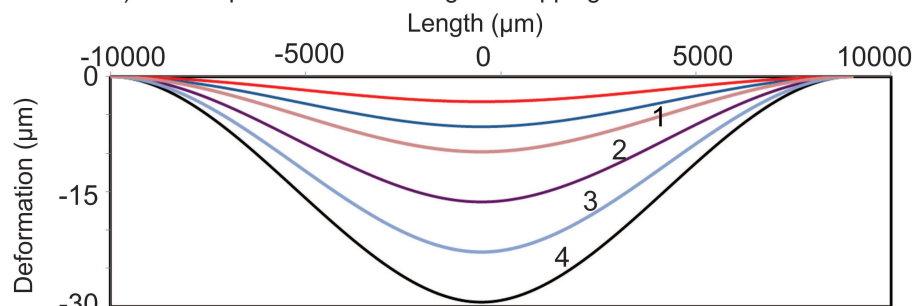
Fig. 3 Experimental results for single-cell trapping. (a) Schematic showing cell trapping via lowering of the push-lens. (b) Image time-sequence showing the trapping of a SYTO green stained lymphoblast cell inside a microcavity. Note that trapping and repositioning of the cell is possible by tuning the CLIC confinement (as demonstrated by the motion of the cell in the time-sequence). (c) Interferometry pattern on the surface of the device corresponds to Newton's rings and determine the location of the push-lens with respect to the nano/micro features and the suction hole. (d) Simulation results represent the chamber height during cell trapping. The inset numbers each correspond to a particular frame in the time sequence in (b): 1 (4.54 s), 2 (4.72 s), 3 (4.74 s) and 4 (4.82 s).

confined area. Here we show that applying vacuum at a through-hole (suction hole) adjacent to the confined area will decrease pressure inside the confinement area and generate sufficient flow to cycle DNA through the confined region.

We use 2D COMSOL creeping flow simulations with no slip-boundary conditions to model flow actuation in our CLIC-based device. The simulation results predict the hydro-dynamic response in the presence of the suction hole. The COMSOL geometry consists of inlet microchannel ($20\,\mu$m-deep), cubic cavity ($100\,\mu$m), micro-loading region ($1\,\mu$m), outlet microchannels ($20\,\mu$m-deep) and a central suction hole ($500\,\mu$m-wide). Fig. 2(a-c) displays fluid flow magnitude for three different operation conditions: (1) with the lid raised and the pressure drop applied betwen the inlet and outlet holes (Fig. 2(a)), (2) with the lid lowered and the pressure drop applied between the inlet and outlet holes (Fig. 2(b)) and (3) with the lid lowered and pressure applied between the inlet and *suction* holes (Fig. 2(c)). Evidently, while lowering the lid suppresses fluid flow in the inlet microchannel and cavity, reducing molecular throughput to the nanochannels (Fig. 2(b)), applying vacuum at the suction hole re-introduces fluid flow in the loading structures, generating sufficient flow to drive extracted DNA from the microcavity into the microloading region and then into the nanochannel array.

Stained λ-phage DNA solution was used to demonstrate the device performance when vacuum is applied through the suction hole. When the push-lens is lowered with no vacuum applied, the DNA molecules are driven out of the nanoconfined region: Fig. 2(e) shows depletion of the DNA molecules in a field of view at the center of the CLIC push-lens. If vacuum is applied, we can reverse the depletion and accumulate DNA in the nanoconfined region: as demonstrated in Fig. 2(d), the number of accumulated DNA molecules inside the nanoconfined region increases with the applied vacuum through suction hole. By increasing the vacuum to almost 6 kPa, we can increase the DNA concentration in nanoconfinement by a factor of five. Fig. 2(f) shows a fluorescence microgram of the nanoconfined region with 6 kPa applied through the suction hole. The suction-based flow actuation mechanism can also be used to deplete the cavity of DNA. When the CLIC lens is lowered, the λ-DNA molecules are trapped inside the cavity due to the high confinement.

3.2 Single-cell trapping

Our CLIC-based micro/nanofluidic device is designed to capture and trap one single cell inside a microcavity via position-
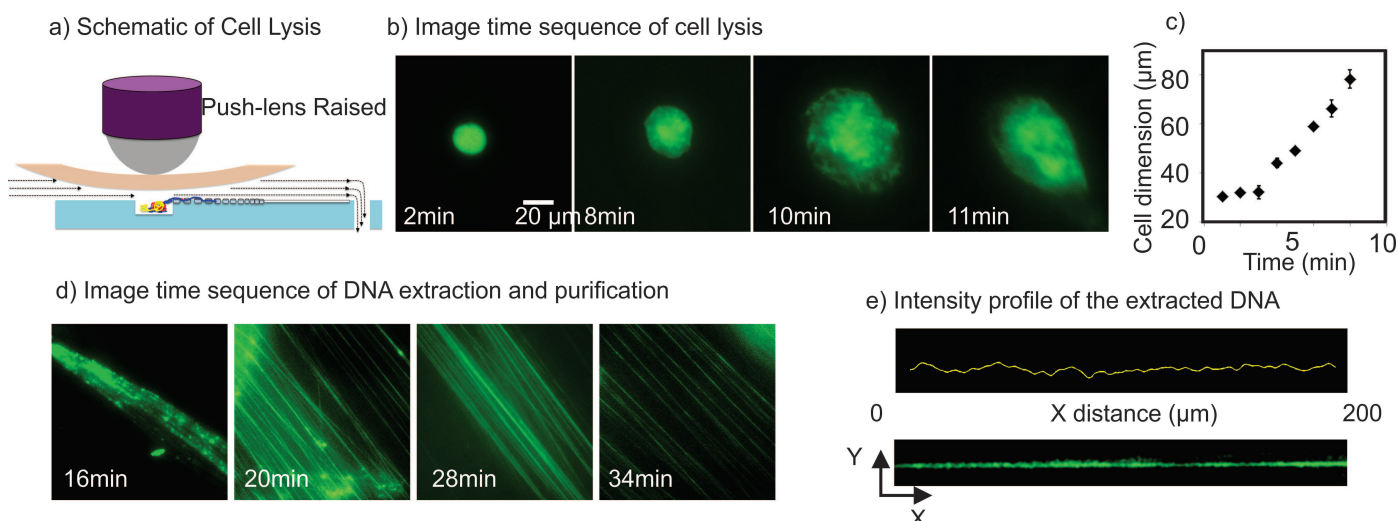
Fig. 4 Experimental results for single-cell lysis and DNA extraction. (a) Schematic showing the cell lysis process in the microcavity. (b) Image time-sequence showing cell lysis proceeding via introduction of RIPA buffer via suction applied at the outlet hole. (c) Cell dimension changes versus time as the cell starts swelling (d) Image time-sequence for genomic DNA extraction. Cellular contents, including genomic DNA and RNA are extracted as time proceeds. The extracted genomic DNA is stained in situ with YOYO-1 added to the buffer. Heating the chamber to $37°C$ activates the proteinase K and dissociates histones and other chromatin proteins from the extracted stands. (e) Intensity profile along one individual DNA showing the continuity and uniformity along the DNA length.

ing of the CLIC push-lens. Prior to loading the cell solution, the center-position of the push-lens is determined using interferometry. Fig. 3c shows the center of the push-lens with respect to the nano/micro patterning on the bottom substrate. Lymphoblastoid cells grown under standard culture conditions are stained with SYTO Green, a cell permeant dye that stains both DNA and RNA (see Materials and Methods). Using a syringe pump, a solution containing stained lymphoblastoid cells was injected into the device and driven to the device center at a flow rate of $4\,\mu$L/min. As the CLIC-based device can be loaded with the lid-raised, we can achieve high loading flow rates, more than 130 times higher than classic microfluidic methods[7,30]. The pressure difference between the inlet and outlet reservoir was measured as 3 kPa using a Extech Heavy Duty Differential Pressure Manometer (5 psi). Syringe pump-actuated hydrodynamics alone is not sufficient to capture single cells in the cavity as the cells will be simply driven across the cavity by the flow. However, we have found that strong localized flows, with speeds of up to $250\,\mu$m/s can be generated by dynamic lowering of the pusher-lens. These flows are in addition confined by the deeper microcavity due to its lower hydraulic resistance. We use this local flow to push a single-cell into the microcavity. Once a cell is trapped in the cavity, the high confinement created by the lowering of the lens then prevents cell escape (see schematic in Fig. 3a). The cell capturing process is monitored using brightfield and fluorescence microscopy as shown in Fig. 3b. The image time sequence shows repositioning of a captured cell ($20\,\mu$m) upon lowering

the push-lens in almost 0.3 s, along with the estimated deflection of the CLIC lid during the repositioning. It is possible to estimate the height of the confined chamber as the push-lens is lowered during cell traping. Fig. 3d. demonstrates the simulation results of the coverslip's deformation upon lowering the push-lens.

Once the cell is trapped, we slightly reduce the confinement, creating a gap sufficient for fluid flow but too small to allow cell escape ($\sim 1\,\mu$m). The buffer is then exchanged (to 100 mM Tris) to remove any remaining cell culture medium or cell debris. With the lid slightly raised, the fluid exchange does not require suction.

3.3 Cell lysis and DNA extraction

Cell lysis is initiated when lysis buffer containing 0.5-2% SDS (see Materials and Methods) is introduced into the microcavity by pumping across the loading reservoirs through the inlet and outlet fluid ports with high flow rate of $2\,\mu$L/min. The lid remains slightly raised (Fig. 4a). The achieved flow rate for loading lysis buffer is much higher than classical microfluidic devices[30], allowing more rapid buffer exchange. The SDS component of the lysis buffer dissolves the cellular and nuclear membranes, eventually releasing the cellular contents including genomic DNA into the microcavity. Figure 4b shows an image time-sequence of the captured cell undergoing chemical lysis: the cell starts swelling 2 min after

a) Schematic of DNA loading in nanochannels

Push-lens Lowered

g)

Lowering push-lens

b) 40 µm

c) 10 µm

d) 10 µm

e) Time 10 µm

f) 20 µm
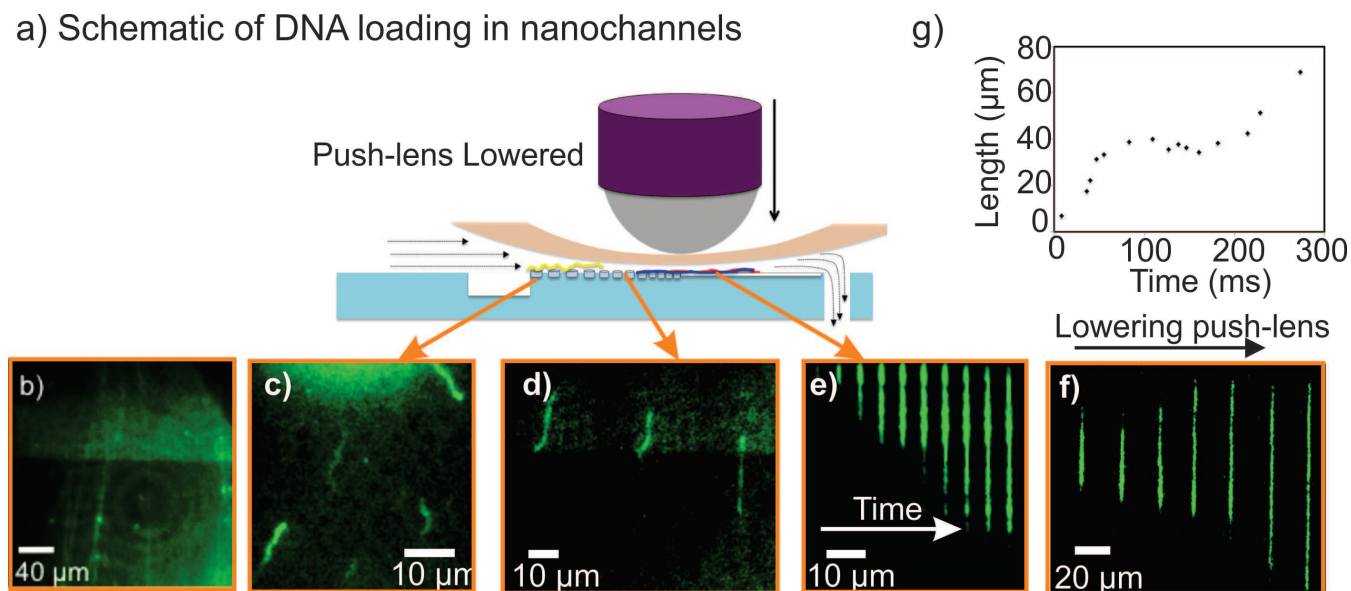
Fig. 5 (a) Cartoon showing DNA loading into the nanochannel array by tuning the confinement. Raising the push-lens helps displacement and fragmentation of genomic DNA strands by mechanical shearing. Fluorescent images show the chamber while (b) the push-lens is raised up to ∼400 nm. (c) Genomic DNA fragments moving along the micropost arrays upon lowering of the push-lens, (d) subsequently enter the nanochannels and (e) then extend along the channels as the height of the CLIC chamber is tuned. (f) Image time-sequence showing one nanochannel confined genomic DNA molecule stretching out as the push-lens is lowered and the CLIC chamber is tuned. (g) Plot of the DNA extension versus time for the molecule shown in (f)

the lysis buffer is introduced, and the cell membrane is eventually completely lysed after 11 min, releasing genomic DNA. Fig. 4c shows the cell dimension versus time during membrane digestion. Within 16 min the cell is completely lysed and YOYO1-stained DNA fibers are clearly visible in the confinement region. At this point suction is applied to increase the flow (6 kPa total drop from inlet to suction hole), leading to the release of long DNA fragments (Fig. 4d). The proteinase K (200 µg/mL) component of our RIPA solution denatures and strips histone proteins from the DNA, converting the chromatin structure into purified DNA strands[7,21]. The device is heated to 37 °C for the most efficient protein digestion[21,30]. The time-sequence images of DNA extraction in Fig. 4d shows the chromatin digestion upon activation of proteinase K, where the genomic DNA strands are revealed in less than 20 min. Increasing the RIPA incubation times tends to remove the non-uniformities. In particular, time-sequence images of Fig. 4d show the DNA state at time-scales of 16-34 min after cell lysis. At this point, the non-uniformities are removed and the confined area contains very long stands of genomic DNA with estimated lengths of up to 200 µm in one field of view (Fig. 4e). The intensity profile in Fig. 4e shows uniformity along the on-chip extracted DNA.

3.4 DNA confinement in the nanochannels

In order to load DNA strands inside the nanochannels, confinement is introduced over the nanochannels by repositioning the push-lens over the array center (schematically shown in Fig. 5a). Suction is continually applied to pull the DNA from the microloading region (microcavity and microposts) into the nanochannels. The performance of the micro post arrays in untangling the DNA strands and stream them into the nanochannels without clogging has previously been demonstrated in bonded-micro/nanofluidic devices[3]. In classic micro/nanofluidic devices, the micropost arrays act as a gradient region in front of the nanochannels and improves entry statistics. However, in our CLIC-based device we have found the action of the push-lens and the ability to modulate confinement *in situ* during DNA entry obviates the need for microposts in our gradient region.

As shown in Fig. 5b-5d DNA molecules are introduced into the nanochannels with the push-lens slightly raised (to a gap height ∼400 nm), lowering the confinement barrier and facilitating DNA entry into the channels. The lid is then lowered once the DNA enters the nanochannels. DNA extension occurs in the nanochannel when the push-lens is in its lowest position (see time-sequence in Fig. 5e and 5f). Using this approach, we successfully confined fragments of

a) Lambda DNA

b) Genomic DNA (250 kbp)

c) Genomic DNA (500 kbp)- one field of view
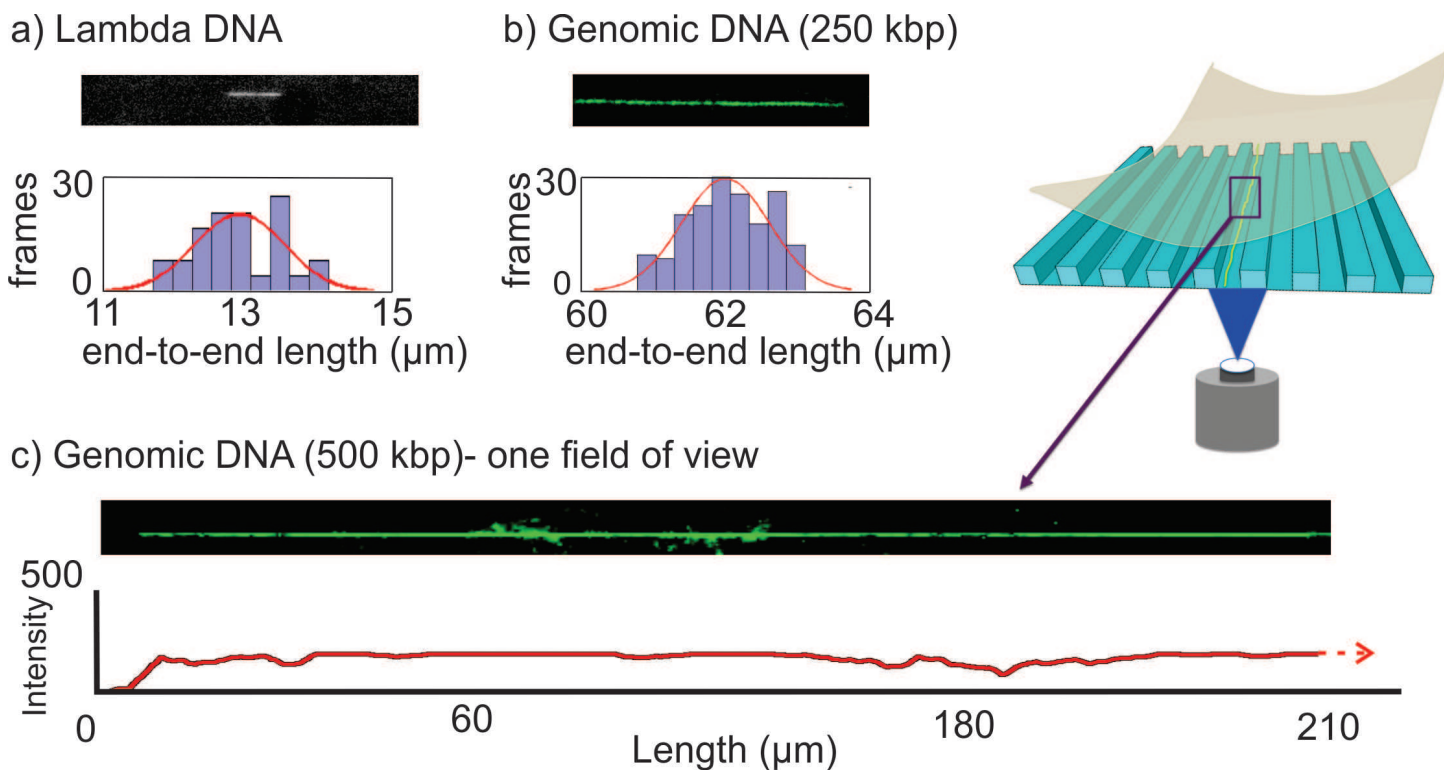
Fig. 6 (a) Representative Lambda DNA molecule and (b) Kilobase genomic DNA extracted from lymphoblast cell confined in 100 nm channel. A single molecule histogram of end-to-end lengths is shown below each image, representing the fluctuations in length throughout a 100-frame movie. (c) Megabase size genomic DNA extracted from lymphoblast cell confined in 100 nm channel

genomic DNA molecules as long as $70\,\mu$m in the nanochannels (Fig. 5g). We have found that if the lowering and raising of the pusher-lens is performed too quickly the resulting flow will tend to fragment the DNA in the microloading region. Consequently, it is very important to find a lowering/rising rate that is a good compromise between gentle DNA handling and rapid operation. Using a lowering/raising rate of 20 nm/sec, which we have found to be optimum, we were able to dramatically increase the fragment size of DNA introduced into the nanochannel array. In particular, using a device with 450μm long nanochannels, we were able to extend a molecule that is three times longer than our field of view (one filled field of view for this fragment is shown in Fig. 6c.). The size of the DNA fragments in our channels can be estimated using the extension of λ-DNA as a calibration standard. The mean length of λ-DNA extended in the nanochannels was measured to be $13\,\mu$m (Fig. 6a), suggesting that the average genomic DNA fragment with extended length of $62\ \mu$m corresponds to a approximate sequence length of $\sim$250 kbp (Fig. 6b). The size of the long fragment is then ~ 1.5 Mbp (using a 130 μm field-of-view for our 60x objective). During image processing, any possible non-uniform backgrounds left by the YOYO-1 or other sources were removed by: (1) capturing

background images where there was no DNA molecules present in the exact device regions where we intended to later image molecules and (2) subtracting this background from subsequently acquired DNA containing images in the same region.

4   Conclusion

In this work, we demonstrate that the CLIC approach can be used to efficiently trap single interphase human lymphoblastoid cells, lyse them *in situ*, extract their genomic DNA and extend the extracted molecules in nanochannels for optical analysis. The ability to dynamically alter the flow-cell dimensions using the CLIC push-lens enables simple and efficient cell trapping and imaging, obviating the need for complicated passive or active microvalving for cell trapping. Moreover, we provided a strategy to overcome the large hydrodynamic resistance required to efficiently bring single-molecule analytes from the pipette-tip to the nanofluidic channels. This allows us to bridge the multiple length scales in creating integrated devices for profiling single genomes extracted from single cells. In addition, we show that the CLIC approach

facilitates loading of very long molecules, enabling introduction of Mbp-long molecules into the arrays. We expect that the method presented in this paper will aid the development of single-cell analysis by combining denaturation mapping, nick-based labeling and other barcode alignment techniques on chip.

5 Acknowledgments

References

1 W. Reisner, N. B. Larsen, A. Silahtaroglu, A. Kristensen, N. Tommerup, J. O. Tegenfeldt and H. Flyvbjerg, *Proc. Natl. Acad. Sci. U.S.A.*, 2010, **107**, 13294–13299.

2 J. Chen, R. V. Dalal, A. N. Petrov, A. Tsai, S. E. OLeary, K. Chapin, J. Cheng, M. Ewan, P.-L. Hsiung, P. Lundquist, S. W. Turner, D. R. Hsu and J. D. Puglisi, *Proc. Natl. Acad. Sci. U.S.A.*, 2013.

3 E. T. Lam, A. Hastie, C. Lin, D. Ehrlich, S. K. Das, M. D. Austin, P. Deshpande, H. Cao, N. Nagarajan, M. Xiao and P.-Y. Kwok, *Nat. Biotechnol.*, 2012, **30**, 771–776.

4 E. Lubeck and L. Cai, *Nat. Method.*, 2012, **9**, 743–748.

5 S. L. Gersen and M. B. Keagle, *The Principles of Clinical Cytogenetics*, Humana Press Inc, Totawa NJ, 2005.

6 E. Vanneste, T. Voet, C. L. Caignec, M. Ampe, P. Konings, C. Melotte, S. Debrock, M. Amyere, M. Vikkula, F. Schuit, J.-P. Fryns, G. Verbeke, T. D'Hooghe, Y. Moreau and J. R. Vermeesch, *Nat. Med.*, 2009, **15**, 577–583.

7 J. J. Benitez, J. Topolancik, H. C. Tian, C. B. Wallin, D. R. Latulippe, K. Szeto, P. J. Murphy, B. R. Cipriany, S. L. Levy, P.D.Soloway and H. G. Craighead, *Lab Chip*, 2012, **12**, 4848–4854.

8 J. Gao, X. . Y. and Z.-L.Fang, *Lab Chip*, 2004, **4**, 47–52.

9 S. Srigunapalan, I. A. Eydelnant., C. A. Simmons and A. R. Wheeler, *Lab Chip*, 2012, **12**, 369–375.

10 LevySakin, *Curr. Opin. Biotech.*, 2013, **24**, 690 – 698.

11 F. Perssona and J. O. Tegenfeldt, *Chem. Soc. Rev.*, 2010, **39**, 985–999.

12 H. Shintaku, H. Nishikii, L. A. Marshall, H.Kotera and J. G. Santiago, *Anal. Chem.*, 2014, **86**, 1953–1957.

13 J. O. Tegenfeldt, C. Prinz, H. Cao, R. L. Huang, R. H. Austin, S. Y. Chou, E. C. Cox and J. C.Sturm, *Anal. Bioanal. Chem.*, 2004, **378**, 1678–1692.

14 H. Yin and D. Marshall, *Curr. Opin. Biotech.*, 2012, **23**, 110–119.

15 Y. Zheng, J. N., Y.Wei and Y. Sun, *Lab Chip*, 2013, **13**, 2464.

16 H. Wu, A. W. and R. N. Zare, *Proc. Natl. Acad. Sci. U.S.A.*, 2004, **101**, 12809–12813.

17 P. Fanzio, V. Mussi, C. Manneschi, E. Angeli, G. Firpo, L. Repetto and U. Valbusa, *Lab Chip*, 2011, 2961.

18 W. Reisner, N. B. Larsen, H. Flyvbjerg, J. O. Tegenfeldt and A. Kristensen, *Proc. Natl. Acad. Sci. U.S.A.*, 2009, **106**, 79–84.

19 P. keng Lin, C.-C. Hsieh, Y.-L. Chen and C.-F. Chou, *Macromolecules*, 2012, **45**, 2920–2927.

20 A. d. B. G. B. Salieb-Beugelaar, K. D. Dorfman and J. C. T. Eijke, *Lab Chip*, 2009, **9**, 2508–2523.

21 R. Marie, J. N. Pedersen, D. L. V. Bauer, K. H. Rasmussen, M. Yusuf, E. Volpi, H. Flyvbjerg, A.Kristensen and K. U. Mir, *Proc. Natl. Acad. Sci. U.S.A.*, 2013, **110**, 4893–4898.

22 Y. Kim, K. S. Kim, K. L. Kounovsky, R. Chang, G. Y. Jung, J. J. dePablo, K. Jo and D. C. Schwartz, *Lab Chip*, 2011, 1721.

23 D. Gupta, J. Sheats, A. Muralidhar, J. J. Miller, D. E. Huang, S. Mahshid, K. D. Dorfman and W. Reisner, *J. Chem. Phys.*, 2014, **140**, 1–8.

24 K. Jo, D. M. Dhingra, T. Odijk, J. J. de Pablo, M. D. Graham, R. Runnheim, D. Forrest and D. C. Schwartz, *Proc. Natl. Acad. Sci. U.S.A.*, 2007, **104**, 2673–2678.

25 L. Dai, J. R. C. van der Maarel and P. S. Doyle, *ACS Mac. Letts.*, 2012, **1**, 732–736.

26 S. R. Leslie, A. P. Fields and A. E. Cohen, *Anal. Chem.*, 2010, **82**, 6224.

27 D. Berard, F. Michaud, S. Mahshid, M. J. Ahamed, M. CMJ, J. S. Leith, P. Brub, R. Sladek, W. Reisner and S. Leslie, *Proc. Natl. Acad. Sci. U.S.A.*, 2014, **111**, 1329513300.

28 M. W. Elting, S. R. Leslie, L. S. Churchman, J. Korlach, C. M. J. McFaul, J. S. Leith, M. J. Levene, A. E. Cohen and J. A. Spudich, *Opt. Express*, 2013, **21**, 1189–1202.

29 W. Reisner, J. N. Pedersen and R. H. Austin, *Rep. Prog. Phys.*, 2012, **75**, 106601–106610.

30 K. H. Rasmussen, R. Marie, J. M. Lange, W. E. Svendsen, A. Kristensen and K. U. Mir, *Lab Chip*, 2011, **11**, 1431–1433.

31 B. C. Kim, C. Moraes, J. Huang, T. Matsuoka, M. D. Thouless and S. Takayama, *Small*, 2014, **10**, 40204029.

32 D. Berard, C. McFaul, J. Leith, A. Arsenault, F. Michaud and S. Leslie, *Rev. Sci. Instr.*, 2013, **84**, 10374–103714.

33 M. J. Ahamed, D. Senkal, A. A. Trusov and A. M. Shkel, *Sensors IEEE*, 2013, **1**, 1–4.

Lab on a Chip Accepted Manuscript